

Approaching the investigation of plasma turbulence through a rigorous verification and validation procedure: A practical example)

P. Ricci, F. Riva, C. Theiler, A. Fasoli, I. Furno, F. D. Halpern, and J. Loizu

Citation: *Physics of Plasmas* (1994-present) **22**, 055704 (2015); doi: 10.1063/1.4919276

View online: <http://dx.doi.org/10.1063/1.4919276>

View Table of Contents: <http://scitation.aip.org/content/aip/journal/pop/22/5?ver=pdfcov>

Published by the [AIP Publishing](#)

Articles you may be interested in

[Generation of a magnetic island by edge turbulence in tokamak plasmas](#)

Phys. Plasmas **22**, 030704 (2015); 10.1063/1.4916580

[A new continuum approach for nonlinear kinetic simulation and transport analysis](#)

Phys. Plasmas **22**, 022301 (2015); 10.1063/1.4906051

[Kinetic Alfvén wave turbulence and formation of localized structures](#)

Phys. Plasmas **20**, 082305 (2013); 10.1063/1.4818506

[Turbulent anomalous transport and anisotropic electron heating in a return current system](#)

Phys. Plasmas **18**, 022308 (2011); 10.1063/1.3553026

[The effect of spectral anisotropy of fast magnetosonic turbulence on the plasma heating at the proton kinetic scales](#)

Phys. Plasmas **17**, 112902 (2010); 10.1063/1.3509158

Did your publisher get
18 MILLION DOWNLOADS in 2014?
AIP Publishing did.



THERE'S POWER IN NUMBERS. Reach the world with AIP Publishing.



Approaching the investigation of plasma turbulence through a rigorous verification and validation procedure: A practical example^{a)}

P. Ricci,^{b),c)} F. Riva, C. Theiler, A. Fasoli, I. Furno, F. D. Halpern, and J. Loizu
*Centre de Recherches en Physique des Plasmas, Ecole Polytechnique Fédérale de Lausanne,
 CH-1015 Lausanne, Switzerland*

(Received 18 November 2014; accepted 6 February 2015; published online 4 May 2015)

In the present work, a Verification and Validation procedure is presented and applied showing, through a practical example, how it can contribute to advancing our physics understanding of plasma turbulence. Bridging the gap between plasma physics and other scientific domains, in particular, the computational fluid dynamics community, a rigorous methodology for the verification of a plasma simulation code is presented, based on the method of manufactured solutions. This methodology assesses that the model equations are correctly solved, within the order of accuracy of the numerical scheme. The technique to carry out a solution verification is described to provide a rigorous estimate of the uncertainty affecting the numerical results. A methodology for plasma turbulence code validation is also discussed, focusing on quantitative assessment of the agreement between experiments and simulations. The Verification and Validation methodology is then applied to the study of plasma turbulence in the basic plasma physics experiment TORPEX [Fasoli *et al.*, *Phys. Plasmas* **13**, 055902 (2006)], considering both two-dimensional and three-dimensional simulations carried out with the GBS code [Ricci *et al.*, *Plasma Phys. Controlled Fusion* **54**, 124047 (2012)]. The validation procedure allows progress in the understanding of the turbulent dynamics in TORPEX, by pinpointing the presence of a turbulent regime transition, due to the competition between the resistive and ideal interchange instabilities. [<http://dx.doi.org/10.1063/1.4919276>]

I. INTRODUCTION

Errors affecting the simulations used to describe the complex plasma dynamics in a tokamak can have far reaching consequences. To limit these errors, which can be due both to mistakes present in the code and to the implementation of a non-sufficiently accurate physics model, there is an increasing motivation in plasma physics to use Verification and Validation (V&V) procedures.^{1–3} V&V is composed by three separate tasks: (i) the *code verification* process, which is targeted to assess that the physics model is correctly implemented in the numerical code, (ii) the *solution verification* procedure, used to estimate the numerical error affecting the simulation results, and (iii) the *validation* procedure, used to assess the consistency of the code results, and therefore of the physics model, with experimental data. The procedure is visualized in Fig. 1. Goal of a V&V procedure is therefore to assess the reliability of our numerical codes and the maturity of the understanding of the physics underlying the dynamics of a plasma.

To perform a code verification, one can² (a) perform simple tests, (b) compare codes with each other (this is known as code-to-code benchmark), (c) quantify the discretization error with respect to a known solution, (d) check the convergence of the numerical result to a known solution, and (e) prove that the numerical solution converges to the analytical one at the rate expected for the numerical scheme (order-of-accuracy tests). As they do not require an

analytical solution, the first two techniques [(a) and (b)] are the simplest to use and, in fact, code-to-code benchmarks are routinely used in plasma physics (see, e.g., Refs. 4–10). While valuable, this exercise is not rigorous as it requires that at least one code is fully verified and, generally, it is very difficult to understand if the difference in the code results is due to discretization errors or to a non-correct implementation of the model. Only the three other approaches [(c)–(e)] are rigorous and, in particular, the

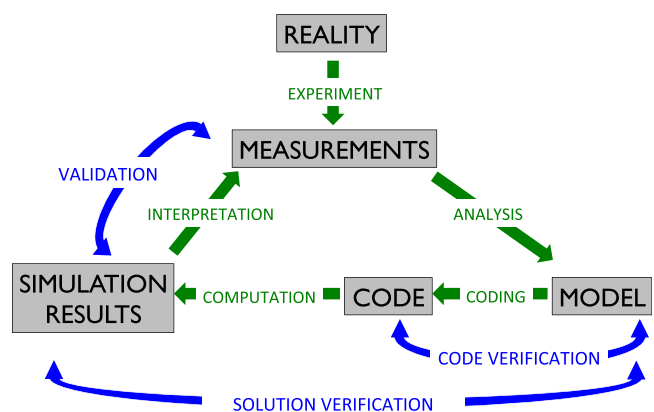


FIG. 1. Schematic representation of the V&V procedure. Through the analysis of experimental data, an analytical model is deduced to describe the evolution of the physical system under consideration. The model equations are then discretized and coded. The simulations results are finally used to interpret the experimental results. Through the code verification procedure, it is assessed that the model equations are correctly implemented in the simulation code. Solution verification allows to estimate the numerical error affecting the simulation results. Finally, the agreement between experiments and simulations is quantitatively assessed through a validation procedure.

^{a)}Paper N12 6, *Bull. Am. Phys. Soc.* **59**, 195 (2014).

^{b)}Invited speaker.

^{c)}Electronic mail: paolo.ricci@epfl.ch

order-of-accuracy test is the only one that can assess quantitatively the correct implementation of the model equations and of the numerical scheme. Order-of-accuracy tests are used in other scientific domains, such as computational fluid dynamics, by using the method of manufactured solution (MMS),^{11–13} which allows order-of-accuracy tests even when an analytical solution is not available for the physics model considered.

Even when a model is correctly implemented in a code, we note that simulations are affected by numerical errors, which should be evaluated through a solution verification procedure.^{2,3,14,15} The sources of numerical error are: (a) round off errors due to the finite number of digits carried over by a computer, (b) statistical sampling errors, (c) errors associated to iterative numerical methods stopped before they reach full convergence, and (d) discretization errors due to the finite grid spacing used by a numerical scheme. While all these errors have to be evaluated, if iterative methods are applied using a sufficiently large number of iterations, and simulations are run long enough to decrease the statistical errors, discretization errors typically dominate over the other sources. Focusing on these errors, for grid-based algorithms, the Richardson extrapolation as higher-order estimator of the solution can be used, as well as the Roache's grid convergence index (GCI) as a relative numerical uncertainty estimate.¹⁶

Guidelines to carry out the validation between experiments and simulations have been ported from other domains, such as computational fluid dynamics, to plasma physics, and are described in Refs. 17 and 18. Simulations and experiments have to be compared considering a number of physical quantities, common to the experimental measurements and simulation results, analyzed using the same techniques. These physical quantities, denoted as validation observables, should be identified and organized into a hierarchy. The latter is based on the number of model assumptions and combinations of measurements necessary to obtain the observable; i.e., how stringent each observable is for comparison purposes. By combining the result of the comparison of all the observables, while taking into account position in the hierarchy and precision, the agreement between simulations and experiments needs to be quantified by using an appropriate composite metric, χ , whose purpose is to quantify the overall agreement between experiments and simulations. The metric χ should be complemented by an index, Q , which assesses the quality of the comparison. Practically, Q provides an indication of the number of observables that have been used for the validation and the strength of the constraints they impose. We remark that the validation should take into account the experimental and simulation uncertainties, therefore these have to be accurately evaluated. Sources of experimental uncertainties are the approximations of the models used to interpret the experimental results, the difficulties in the evaluation of the properties of the measuring devices, and the non-perfect reproducibility of the experiments. For the simulations, uncertainties are due to the numerical error (evaluated through the solution verification procedure) and the uncertainty associated to the non-well known input

parameters. The latter can be estimated through a sensitivity analysis.

We point out that the validation procedures should remain simple. The goal is not mathematical rigor, but a useful tool that can be easily applied in order to compare different models with experimental results. Through this comparison, it is possible to assess the physics elements that play a role in the dynamics of the system and that should be taken into account for its description. On the other hand, it is very delicate to judge a single model in absolute terms in view of testing its predictive capabilities and this is not a subject of the present paper.

Goal of the present paper is twofold. First, we summarize the methodology to carry out the procedures of code verification, simulation verification, and validation. Second, we describe the V&V effort that we have carried out in the recent years to study the plasma dynamics in the basic plasma physics experiment TORPEX^{19,20} by using the GBS code.²¹ This application exemplifies the application of this methodology. Owing to its detailed diagnostics, possibility of parameter scans, and relative simple configuration, TORPEX is an ideal testbed to perform experiment/simulation comparisons and to investigate the corresponding methodological framework. For its simulation, three models have been considered, all based on the drift-reduced Braginskii equations: (a) a three-dimensional two-fluid model, able to describe the global evolution of TORPEX plasma,^{22,23} (b) the same three-dimensional model completed by an appropriate first-principle set of boundary conditions that has been recently derived,²⁴ and (c) a reduced two-dimensional two-fluid model,^{25,26} able to describe only the evolution of $k_{\parallel} = 0$ modes. The three models are implemented in the GBS code. We therefore discuss the verification of the GBS code and of its results. We then compare the simulation results with the experimental results, showing that the validation metric is able to point out that the agreement of the two-dimensional model and the experiment is no longer satisfactory when $k_{\parallel} \neq 0$ modes are present in the experiment. We note that the present work summarizes the results contained in Refs. 27–29 and extend them to the validations of the simulations with the new set of boundary conditions that have been implemented in GBS.

The paper is structured as follows. After the Introduction, we describe the V&V methodology in Sec. II. The application of the methodology to the analysis of the basic plasma physics experiment TORPEX is described in Sec. III. The Conclusions follow. In the Appendixes, we present the details of the TORPEX experimental setup (Appendix A) and of the simulation approach (Appendix B).

II. THE VALIDATION AND VERIFICATION METHODOLOGY

A. Code verification methodology

The order-of-accuracy test can ensure the correct implementation of the physical model and of the numerical scheme.² This test analyzes the convergence of the numerical solution to a known analytical solution, verifying that the discretization errors reduce at the rate expected for the

numerical scheme, as the spatial mesh and the time step are refined.

Given a theoretical model M with an analytical solution s , such that $M(s) = 0$, and the numerically discretized model of M , M_h , with a numerical solution s_h that satisfies $M_h(s_h) = 0$ (h is a parameter representing the degree of refinement of the mesh), the error affecting the numerical results is expressed as $\epsilon_h = \|s_h - s\|$, where $\|\cdot\|$ denotes a designed norm. The theoretical order of accuracy, p , associated with the numerically discretized operator M_h , represents the rate at which the numerical solution converges to the analytical solution as the mesh is refined. The numerical error, in fact, satisfies the relation $\epsilon_h = C_p h^p + O(h^{p+1})$, where C_p is independent of h , and p is the order of accuracy of the numerical scheme, typically evaluated through its Taylor expansion.^{2,3,13} Having the two numerical solutions of M_h and M_{rh} , i.e., s_h and s_{rh} , where rh indicates coarsening the h mesh by a factor r , one can evaluate the observed order of accuracy, p , using

$$p = \frac{\ln(\epsilon_{rh}/\epsilon_h)}{\ln(r)}. \quad (1)$$

If p converges to p for $h \rightarrow 0$, i.e., when the discretization error is dominated by the lowest order term in the expansion (the so-called asymptotic regime), we can state that the code is verified and the equations are correctly solved, with the order of accuracy expected for the numerical scheme.

The main issue related to the systematic evaluation of p is the need of the analytical solution s , necessary to compute the numerical error ϵ_h ; in fact, the analytical solution is unknown in most cases. The MMS, developed to overcome this problem,^{11–13} instead of solving analytically a theoretical model, suggests to impose a solution to the model, the so-called manufactured solution, and to modify the model equations to accommodate the imposed solution; we then numerically solve the obtained modified model to compute the discretized error. More precisely, for a given model M , we choose an analytical function u and we compute a source term, $S = M(u)$, which is subsequently subtracted from M to obtain a new analytical model $G = M - S$, whose analytical solution is u [in fact, $G(u) = M(u) - S = 0$]. The discretization of the new model is straightforward, i.e., $G_h = M_h - S$. Since the source term S is computed analytically, we do not add any new discretization errors to the numerical model considered and, consequently, the behavior of the numerical error is preserved. This can be expressed as: $\epsilon_h = \|u_h - u\| = D_p h^p + O(h^{p+1})$. From a practical point of view, using the MMS for an order-of-accuracy test implies adding source terms to the discretized equations, performing a simulation scan to obtain the observed order of accuracy, and comparing the observed order of accuracy to the theoretical one to verify the code.

Although the idea behind the MMS is trivial, its implementation requires to consider some subtleties. In fact, the manufactured solution should satisfy the following requirements: (a) be smooth enough and not singular, (b) be general enough to excite all the terms present in the equations, (c)

satisfy the code constraints (e.g., positivity for the density or the temperature), and (d) ensure that the magnitude of the different terms composing the equations are of the same order of magnitude. Due to these constraints, the manufactured solutions are usually built as a combination of trigonometric and/or hyperbolic functions; the code verification is in fact a purely mathematical issue and, consequently, as the physics of the problem does not concern the manufactured solutions, no physical constraint is applied on the choice of the analytical functions. We finally note that the MMS cannot be applied to codes used to model singularities, shocks, or discontinuities; the verification of these codes is still an open issue.²

B. Solution verification methodology

Due to finite computational power and the finite precision achievable, the simulation results are always affected by numerical errors, even if the model equations are implemented correctly. Estimating the amplitude of the numerical errors is crucial to ensure the reliability of the numerical results and their magnitude is needed to perform a rigorous validation of the physical model with experimental results. The estimate of the numerical error affecting the simulations constitutes the solution verification procedure.^{2,3,14,15}

The numerical errors affecting a simulation have four sources: round-off errors, iterative errors, statistical sampling errors, and discretization errors.^{2,3} We focus on the discretization errors, introduced by the numerical scheme used to discretize the physical model over a finite mesh, in time and in space.

In the early 20th century, Richardson developed a method,^{30,31} later extended,^{32,33} to accelerate the rate of convergence of a numerical sequence. This method is based upon the use of two numerical solutions obtained using two different meshes, s_h and s_{rh} , to compute an estimate of the analytical solution that presents a convergence rate one order higher than the original numerical solution. Concretely, the Richardson extrapolation is defined as

$$s = s_h + \frac{s_h - s_{rh}}{r^p - 1}, \quad (2)$$

where p is the formal order of accuracy defined in Sec. II A. Noting that $\|s_h - s\| = C_p h^p + O(h^{p+1})$, it follows that the extrapolated solution s satisfies $\|s - s\| = D_p h^{p+1} + O(h^{p+2})$; therefore, for $h \rightarrow 0$, $s \rightarrow s$ faster than the numerical solutions obtained from the simulations. Consequently, we can use s as an estimate of the exact solution s , and approximate the numerical error with the expression

$$\epsilon_h \simeq \|s_h - s\| = \left\| \frac{s_h - s_{rh}}{r^p - 1} \right\|. \quad (3)$$

The relative discretization error, *RDE*, is therefore approximated as

$$RDE = \frac{s_h - s}{s} \simeq \frac{s_h - s}{s} = \frac{s_{rh} - s_h}{s_h r^p - s_{rh}}. \quad (4)$$

For s to be a reasonable estimate of s , however, several assumptions should be satisfied. First, the Richardson

extrapolation method requires the use of uniform mesh spacing, meaning that the degree of the refinement of the meshes can be represented solely by the parameter h discussed before. Therefore, s_h and s_{rh} should be computed over two meshes that are one the uniform systematic refinement of the other, and consequently the application of Richardson extrapolation to computations involving local mesh refinement or mesh adaptation is not allowed. Second, the simulations used to evaluate s should be in the asymptotic regime, meaning that the discretization error is dominated by its lower order term, $C_p h^p$. This requirement could result in computationally very expensive simulations, due to the potential need of very fine meshes. Third, to apply the method presented above for the estimate of the numerical error, the solutions should be smooth enough, with no singularities and/or discontinuities. As a matter of fact, to allow the expansion of the numerical error in term of powers of the parameter h , the derivatives of the analytical solution should exist and be continuous. Moreover, we should note that we do not have any guarantee that the Richardson extrapolated solution meets the same governing equations satisfied by either the numerical solution or the analytical solution; consequently, we use this extrapolation for the computation of the numerical error only.

Usually, it is problematic to satisfy the requirement of being in the asymptotic regime, due to the high computational cost of the simulations. Moreover, it has to be demonstrated that the numerical solutions are in the asymptotic regime, by showing that the observed order of accuracy matches the formal one. This requires at least three simulations, resulting from two subsequent refinements of the coarser mesh of a factor r , from which the observed order of accuracy can be evaluated as

$$p = \frac{\ln[(s_{r^2h} - s_{rh}) / (s_{rh} - s_h)]}{\ln(r)}. \quad (5)$$

If only two simulations are available, or if the observed order of accuracy does not match the formal one, we should substitute the numerical error estimates in Eqs. (3) and (4) with a numerical uncertainty quantification. As a matter of fact, in general, the error estimates in Eqs. (3) and (4) may depend strongly on the refinement factor r and on the precision of the numerical scheme; it is therefore difficult to rely on such error estimate. To overcome these issues, Ref. 16 introduces the GCI defined as

$$GCI = \frac{F_s}{r^p - 1} \left| \frac{s_{rh} - s_h}{s_h} \right|, \quad (6)$$

that represents an estimate of the relative discretization error affecting the simulation results. The GCI value is obtained by approximating in Eq. (4) $s_h r^p - s_{rh} \simeq (r^p - 1)s_h$. The factor of safety F_s and p ensure that GCI is larger than the numerical discretization error in 95% of the cases. Oberkampf and Roy² propose the following: if $|p - p| < 0.1p$, we can assume that the simulation is in the asymptotic regime and we use $F_s = 1.25$, as well as $p = p$. If $|p - p| > 0.1p$, a more conservative factor of safety, $F_s = 3$, has to be used and

$p = \min[\max(0.5, p), p]$. If p is not evaluated (for example, if only two solutions are available), $F_s = 3$ and $p = p$ are used. We remark that, although these definitions are reasonable, there still is an ongoing discussion in the verification community about their generality.

To conclude our presentation of the error estimate methodology, we have to discuss a few details. First of all, we draw the attention to the fact that the present procedure can be applied not only to point-by-point solution values, but also to solution functionals. This is an important point to estimate the numerical error affecting the observables used in the validation of the physical model.³ Second, as s_h and s_{rh} are in general computed on different meshes, the results on the coarser mesh have to be interpolated on the finest grid, using an interpolation scheme whose order is equal or higher than the order of the numerical scheme used by the code. A complete discussion of this topic is found in Ref. 32. Third, using GCI as an evaluation of the numerical error requires a non-oscillatory convergence of the numerical solution. If oscillatory convergence is observed, the numerical error has to be evaluated from the difference between the obtained numerical solutions. Finally, we illustrate a useful propriety of GCI , which is the possibility of computing the overall GCI analyzing each coordinate of the problem independently. As it can result numerically very expensive to perform a uniform refinement of the grid along all the coordinates at the same time, it is possible to refine separately each coordinate of the mesh by a factor r_i , where the index i refers to the coordinate under investigation. This allows us to compute a GCI_i and a p_i for the i coordinate, and obtain the overall GCI as $GCI = \sum_i GCI_i$.

C. Validation methodology

Simulations and experiments have to be compared considering a number of physical quantities, common to the experimental measurements and simulation results, and analyzed using the same techniques. These physical quantities are denoted as validation observables. In order for an observable to be considered, it should satisfy the following criteria. First, the observable should be physically relevant: i.e., focus should be put on observables containing the most important theoretical predictions. Second, each observable should be independent of the other observables. Third, the resolution of the observables should be sufficient to well describe their variation.

Once the observables are defined and evaluated, the agreement between experiments and simulations relative to each observable has to be quantified. We denote with e_j and s_j the values of the j -th observable used in the comparison, as coming from the experimental measurement or the simulation results, respectively. Most of the observables depend on space and time and are typically given on a discrete number of points, denoted as N_j . We denote with $e_{j,i}$ and $s_{j,i}$ the values of the j -th observable at points $i = 1, 2, \dots, N_j$ (the present notation can therefore be used for zero-, one-, two-, etc., dimensional observables). For the j -th observable, we normalize the distance d_j between experiments and simulations with respect to the uncertainty related to these quantities

$$d_j = \sqrt{\frac{1}{N_j} \sum_{i=1}^{N_j} \frac{(e_{j,i} - s_{j,i})^2}{\Delta e_{j,i}^2 + \Delta s_{j,i}^2}}, \quad (7)$$

where $\Delta e_{j,i}$ and $\Delta s_{j,i}$ are the uncertainties related to the evaluation of $e_{j,i}$ and $s_{j,i}$. Since simulations and experiments can be considered to agree if their difference is smaller than their uncertainties, we define the level of agreement between experiments and simulations with respect to observable j as

$$R_j = \frac{\tanh[(d_j - 1/d_j - d_0)/\lambda] + 1}{2}, \quad (8)$$

with $R_j \leq 0.5$ corresponding to agreement (within the experimental and simulation uncertainties), while $R_j \geq 0.5$ denoting disagreement (outside the experimental and simulation uncertainties). Here, we choose $d_0 = 1$ and $\lambda = 0.5$; our tests show that the conclusions of a validation exercise are not affected by the specific choices of the parameters d_0 and λ , if these parameters are within the reasonable range that point out agreement between experiments and simulations when they fall within their uncertainties. Some authors prefer to normalize the distance between experimental and simulation results to the actual value of the observables, rather than to their uncertainty.² We believe that the normalization to the uncertainty is the most appropriate choice in the present case, as we are interested in understanding if the basic physics mechanisms at play in the system are well captured by the model under consideration. The normalization to the actual value of the observable is instead preferable in the case that the predictive capabilities of the code are tested.

Particular attention should be paid in evaluating the experimental and the simulation uncertainties. In the case of the experiments, we can identify three main uncertainty sources. First, the model of a measuring device provides predictions through which one can infer the physical quantities of interest (e.g., from the I-V curve of a Langmuir probe one can infer n and T_e). Experimental measurements typically do not follow perfectly the model predictions: thus, a fit has to be made in order to evaluate the relevant physical parameters, introducing an uncertainty that we denote with $\Delta x_{j,i}^{fit}$. Second, a source of uncertainty is due to properties of the measuring device that are often difficult to evaluate accurately (e.g., geometry and surface condition of a Langmuir probe). Thus, measurements should be performed with different tools (e.g., Langmuir probes which differ in dimension, surface condition, and electronics). The quantity $\Delta x_{j,i}^{prb}$ denotes the uncertainty related to the probe properties. Finally, the plasmas are not perfectly reproducible due to control parameters difficult to set or know precisely (e.g., the vacuum pressure). Experiments should be repeated in order to check the reproducibility of the plasma, while measurements are taken with different measurement devices. The quantity $\Delta x_{j,i}^{rep}$ is the uncertainty due to the plasma reproducibility, averaged over the different measuring devices. The total experimental uncertainty is given by $\Delta x_{j,i}^2 = (\Delta x_{j,i}^{fit})^2 + (\Delta x_{j,i}^{prb})^2 + (\Delta x_{j,i}^{rep})^2$.

Simulations are also affected by uncertainties resulting from two sources: (i) errors due to the numerics (e.g., due to the limited accuracy of the numerical integration scheme

used or due to the finite grid resolution) and (ii) errors due to unknown or imprecise input parameters. While errors due to the numerics, $\Delta y_{j,i}^{num}$, can be estimated through the methodology described in Sec. II B, the evaluation of the error related to not perfectly known input parameters, $\Delta y_{j,i}^{inp}$, requires a uncertainty propagation study, i.e., an investigation of how the model results are affected by the input parameter variations. The number of input parameters of a turbulence simulation code is usually quite large and a complete study of the model response is prohibitive. However, the theory can indicate to which input parameters the results are particularly sensitive. The analysis has then to focus on those. We remark that in the literature, a number of useful techniques have been proposed to predict the response of the model to variation of simulation parameters using the smallest possible number of simulations (see, e.g., Ref. 34). As in the case of the experimental error bars, the two sources of error should be added, such that $\Delta y_{j,i}^2 = (\Delta y_{j,i}^{num})^2 + (\Delta y_{j,i}^{inp})^2$.

We note that the error bars should not take into account the uncertainties related to model assumptions and/or to combinations of measurements, which are often needed to deduce the comparison observables from the simulation results and the raw experimental data.²⁷ Evaluating rigorously those uncertainties is usually very challenging. The idea is to take them into account approximately through the observables primacy hierarchy. More specifically, the higher the hierarchy level of an observable is, the lower the importance of the observable in the comparison metric.

The overall level of agreement between simulations and experiments can be measured by considering a composite metric, which should take into account the level of agreement of each observable, R_j , and weight it according to how constraining each observable is for comparison purposes. This means that the hierarchy level of each observable and the level of confidence characterizing the measurement or the simulation of each observable have to be considered. The higher the level in the primacy hierarchy and the bigger the error affecting the observable measurement, the smaller the weight of the observable should be. We thus define the metric χ as

$$\chi = \frac{\sum_j R_j H_j S_j}{\sum_j H_j S_j}, \quad (9)$$

where H_j and S_j are functions defining the weight of each observable according to its hierarchy level and the precision of the measurement, respectively. Thanks to the definition of R_j , χ is normalized in such a way that perfect agreement is observed for $\chi=0$, while simulation and experiment disagree completely for $\chi=1$.

The definition of H_j and S_j is somewhat arbitrary. H_j should be a decreasing function of the hierarchy level. The definition we adopt is $H_j = 1/h_j$, where h_j is the combined experimental/simulation primacy hierarchy level, which takes into account the number of assumptions or combinations of measurements used in evaluating the observables both from the experiments and from the simulations. In

practice, if no assumptions or combinations of measurements are used for obtaining an observable, $h_j = 1$, any assumption or combination of measurement leads h_j to increase of a unity (see Ref. 27 for more details on the h_j definition). The quantity S_j should be a decreasing function of the experimental and simulation uncertainty. We introduce the following definition:

$$S_j = \exp \left(- \frac{\sum_i \Delta e_{j,i} + \sum_i \Delta s_{j,i}}{\sum_i |e_{j,i}| + \sum_i |s_{j,i}|} \right), \quad (10)$$

such that $S_j = 1$ in the case of zero uncertainty.

The validation metric should be complemented by an index, Q , that assesses the “quality” of the comparison. The idea is that a validation is more reliable with a larger number of independent observables, particularly if they occupy a low level in the primacy hierarchy and the measurement and simulation uncertainties are low. The quality of the comparison Q can thus be defined as

$$Q = \sum_j H_j S_j. \quad (11)$$

III. EXAMPLE OF APPLICATION OF THE VALIDATION AND VERIFICATION METHODOLOGY

We present an example of V&V procedure, where we apply the methodology described in Sec. II. We discuss the simulations of plasma turbulence in the basic plasma physics experiment TORPEX^{19,20} that have been carried out with the GBS code. The GBS code has been developed in the last few years to simulate plasma turbulence in the open field region of magnetic confinement devices, evolving the drift-reduced Braginskii two-fluid equations,³⁵ without any separation between equilibrium and perturbation quantities.²¹ In the development of the GBS code, increasingly complex magnetic configurations have been considered: first, the code was developed to describe basic plasma physics devices, in particular, linear devices such as LAPD³⁶ and simple magnetized toroidal devices such as TORPEX,²³ whose simulations are the focus of the present paper. GBS was then extended to the tokamak geometry, and it is now able to model the tokamak scrape-off layer (SOL) region in limited plasmas (see, e.g., Refs. 37–40). GBS has been subject of a rigorous code verification procedure described in Ref. 29 that we briefly summarize in Sec. III A.

TORPEX features a simple magnetized plasma, in a toroidal configuration of major radius R and height L_v , where a vertical magnetic field, B_z , superimposed on a toroidal magnetic field, B_ϕ , creates helicoidal field lines winding around the device.^{19,20} Pressure gradients and magnetic curvature drive a number of instabilities that develop into turbulence and lead to transport of heat and particle across the magnetic field lines,⁴¹ while the plasma flows along them to be lost at the vessel walls. The TORPEX experimental setup and the Langmuir probe diagnostics used (HEXTIP, SLP, and TWIN) are described in Appendix A. We remark that the

TORPEX experimental setting is particularly suited for experiment/simulation comparison, thanks to its detailed diagnostics, the possibility of performing easily parameter scans, and relatively simple geometry, which allows global simulations particularly suited for a detailed comparison.

For the comparison of simulations and experiments, we consider a set of TORPEX configurations with different values of vertical magnetic field, characterized by different properties of plasma turbulence. We analyze four scenarios, characterized by different windings of the magnetic field lines, i.e., $N = 2, 4, 8$, and 16 , being $N = L_v B_\phi / (2\pi R B_z)$ the number of field line turns in the device. By using GBS, we carry out simulations of TORPEX plasma turbulence by considering three different models: (a) a global three-dimensional two-fluid model that describes the evolution of the plasma dynamics in the full TORPEX volume, (b) a global three-dimensional two-fluid model that describes the evolution of the plasma dynamics in the full TORPEX volume provided with first-principle boundary conditions recently derived,²⁴ and (c) a two-dimensional model that is able to represent only $k_\parallel = 0$ modes. The details of the simulation models as well as the simulation input parameters are described in Appendix B. As described in Sec. III B, we verify the solution of the GBS code, estimating the numerical error that affects the validation observables, and we carry out a rigorous validation exercise, as described in Sec. III C.

A. Code verification

GBS has been subject to the code verification procedure described in Ref. 29. Here, we recall the main elements of the procedure. To verify the implementation of the drift-reduced Braginskii equations into GBS and to satisfy the requirements given in Sec. II A, we choose to manufacture the model solution as the combination of trigonometric functions, with the amplitude of the coefficients such that, for the used meshes, the simulations are in the asymptotic regime and the errors affecting the different terms are of the same magnitude.

The computation of the source terms S is trivial: it consists in plugging the analytical manufactured solutions into the drift-reduced Braginskii equations. This process is particularly tedious, but it involves only straightforward algebraic manipulations with no conceptual difficulties and can be carried out by using the symbolic manipulation software *Mathematica*,⁴² which allows the direct translation into the *Fortran* language in which GBS is written. This enables the implementation of the obtained expressions in GBS, without any significant difficulty and reducing the possibilities of mistakes.

In Ref. 29, we report the results of the code verification. The numerical error, evaluated as the norm of the difference between the numerical and the manufactured solutions, decreases with the grid spacing linearly on a logarithmic scale, when refining the mesh, with the slope expected from the order of accuracy of the numerical method. The scan we perform shows a reduction of the numerical error by at least three orders of magnitude, giving confidence that there are

not subdominant errors decreasing at a rate different than the expected one.

B. Solution verification

The estimate of the numerical error affecting a simulation is needed not only to ensure the reliability of the numerical results, but also to perform the validation of the physical model. It is therefore a fundamental step in the V&V procedure. In this subsection, we apply the approach presented in Sec. II B to the GBS code to exemplify the procedure and to assess the numerical error affecting the TORPEX simulations.

A previous solution verification procedure applied to the GBS code²⁹ shows that the numerical error affecting the simulations is mostly due to the space discretization, while the time discretization leads to a negligible numerical error. We therefore perform three simulations of TORPEX turbulence for $N=2$ by increasing the spatial grid resolution in all directions, focusing our attention on the numerical error that affects the ten validation observables considered in Sec. III C. In particular, we consider the equilibrium radial

profiles at the vertical midplane of density, n , electron temperature, T_e , electric potential, ϕ , ion saturation current, I_{sat} , normalized I_{sat} fluctuations, $\delta I_{sat}/I_{sat}$, I_{sat} skewness, and kurtosis. We also use as validation observables the value of the vertical wavenumber, k_z , the Probability Distribution Function (PDF), and the Power Spectrum Density (PSD) of I_{sat} at the vertical midplane, at the radial point where I_{sat} is equal to the 3/4 of its peak value (this is the location where we expect to identify more clearly the turbulence properties). We plot the results of the three simulations in Fig. 2. Convergence in some cases shows an oscillatory character: as the necessary condition to use the *GCI* estimate are missing, we estimate the numerical uncertainty as the spatial average of the maximum of the relative difference between the different simulations. The errorbar associated with this uncertainty is plotted in Fig. 2.

C. Validation

To compare experiments and simulations, we use measurements obtained by Langmuir probes. A number of observables have been identified based on Langmuir probe

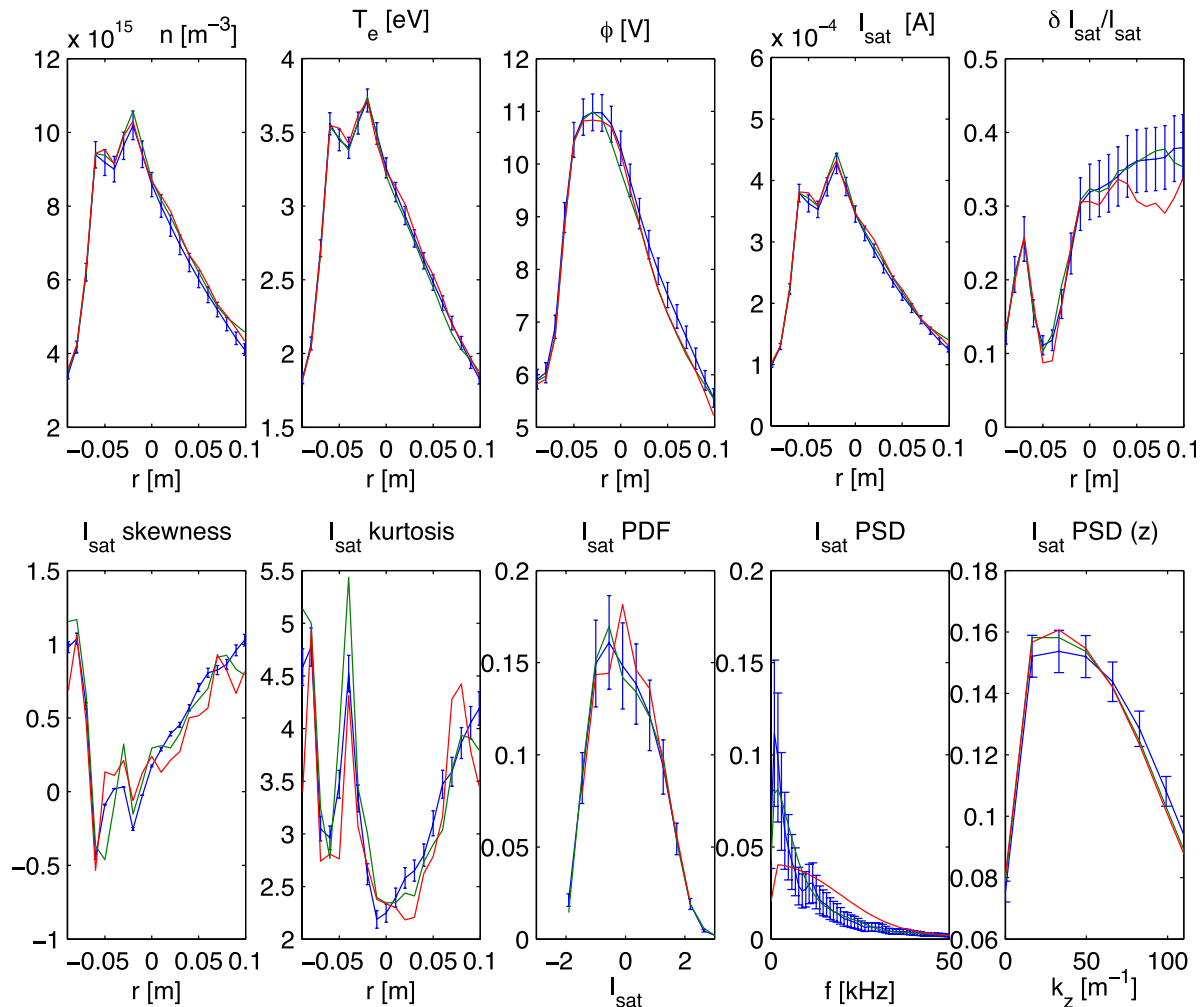


FIG. 2. Evaluation of the numerical uncertainty due to the numerical discretization. The ten observables considered for the validation procedure are plotted for TORPEX simulations with $N=2$, considering an increasing refinement of the mesh: $N_r \times N_z \times N_\phi = 128 \times 128 \times 32$ (blue), $N_r \times N_z \times N_\phi = 192 \times 192 \times 48$ (green), and $N_r \times N_z \times N_\phi = 288 \times 288 \times 72$ (red). The resulting estimated uncertainty is represented by the errorbars. The I_{sat} PDF is rescaled to the same values of average, variance, and area. The PSD is rescaled to the same area.

TABLE I. Primacy hierarchy for some observables obtained from Langmuir probe measurements. The experimental hierarchy counts the number of assumptions or combinations of measurements used to obtain the observables from experimental data (the first level in the hierarchy denotes no assumptions or combinations of measurements; then, each assumption or combination of measurements increases the hierarchy level of a unity). The same definition is used for the simulation hierarchy. The comparison hierarchy sums the experimental and simulation assumptions.

	Experimental hierarchy	Simulation hierarchy	Comparison hierarchy
Moments, PDF, and PSD of I_{sat} and V_{fl}	1	2	2
T_e , \mathbf{w} , ϕ	2	1	2
Results from spectral analysis (e.g., k_z)	2	1	2
Statistical analysis of turbulent structures	2	3	4
T_e	3	1	3
Particle flux	3	2	4

measurements^{27,43} and we list them in Table I; herein, we use the ten observables at the second level of the comparison hierarchy ($H=0.5$ in all cases) that are mentioned in Sec. III B. For each observable, the experimental uncertainty Δx is evaluated by repeating the experiments a number of times, and comparing the measurements of different probes. The simulation uncertainty, Δy , is evaluated by performing a number of simulations where we vary the input parameters. A complete sensitivity scan would require the analysis of all input parameters; however, due to the high computational

cost of the present simulations large parameter scans are prohibitive at the moment, and we have focused our attention on the parameters that are expected to most significantly affect the simulations and that are not well known. For the three-dimensional simulations, these are the plasma resistivity ν and the boundary conditions (in the case of simulations with ad hoc boundary conditions). An example of uncertainty evaluation is shown in Fig. 3, where we show three simulations carried out with different values of ν and the errorbar we deduce. For the two-dimensional simulations, instead, we

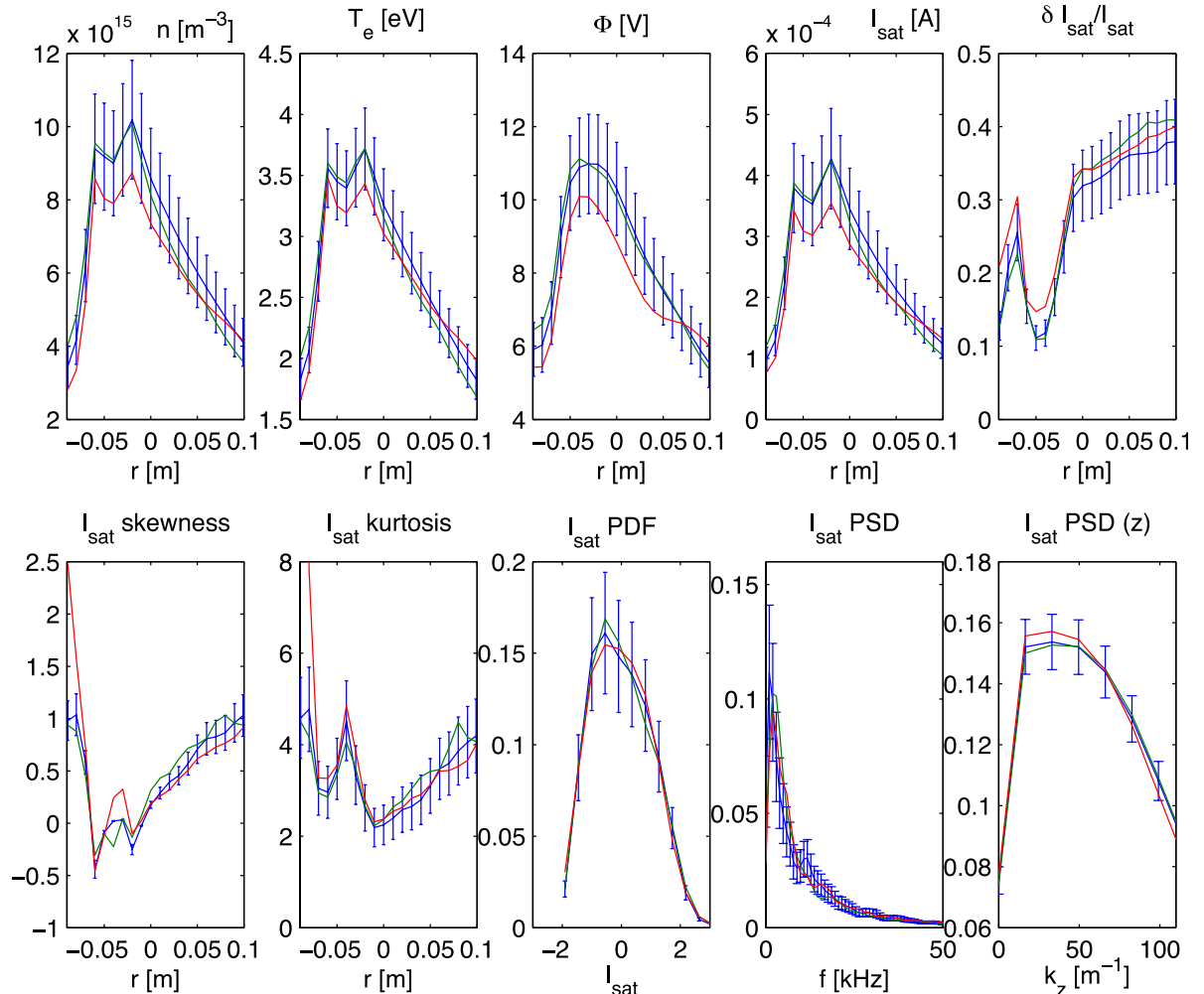


FIG. 3. Evaluation of the numerical uncertainty due to poorly known input parameters (in this case plasma resistivity). The ten observables considered for the validation procedure are plotted for TORPEX simulations with $N=2$, considering $\nu = 0.01$ (green), $\nu = 0.1$ (blue), and $\nu = 1$ (red). The resulting estimated uncertainty is represented by the errorbars. The I_{sat} PDF is rescaled to the same values of average, variance, and area. The PSD is rescaled to the same area.

study the sensitivity to the parameter describing the parallel losses, σ , that is introduced in Appendix B.

The values of χ are plotted in Fig. 4, which describes the dependence of the simulation/experiment agreement as a function of the number of field line turns, N , for both the two-dimensional and three-dimensional simulations, with and without the first-principle set of boundary conditions). For the three-dimensional simulations, it is $\chi \simeq 0.5$, showing that the three-dimensional simulations are able to represent equally well low and high N scenarios. A clear trend is instead observed in the case of the two-dimensional simulations, where the agreement decreases with N , passing from $\chi \simeq 0.6$ for $N=2$ to $\chi \simeq 0.9$ (i.e., almost complete disagreement) for $N=16$. With respect to the observables considered herein, no clear improvement is observed in the simulations carried out with the first-principle set of boundary conditions.

If we look at the origin of the discrepancy between simulations and experiment in more details, we observe that the three-dimensional simulations generally describe reasonably well the equilibrium profiles of n , and I_{sat} . The agreement is worse in the case of the T_e and ϕ profiles. A significant discrepancy between simulations and experiments is revealed by the comparison of the turbulence amplitude levels, as the simulated turbulence amplitude is about a factor of two smaller than the experimental one. The analysis of the PSD reveals that the difference between the experimental and simulated turbulence level is present across all the frequencies.

For two-dimensional simulations, agreement strongly decreases with increasing N for the majority of the observables. In fact, for $N=2$ and $N=4$, the agreement between two-dimensional simulation and experiment is comparable to the one observed in the case of three-dimensional simulations. The agreement strongly decreases at higher N , and at $N=16$ all the observables reveal a complete disagreement.

The quality of the comparison is also plotted in Fig. 4. Since the uncertainties for all the observables are relatively small and all the observables are at the second level of the validation hierarchy, Q is about constant as a function of N , and in particular, $Q \simeq 4$, that is close to the maximum value, $Q=5$ that can be obtained by using 10 observables at the second level of hierarchy. The Q values reported in the present validation project can be compared with the Q that would be obtained in a validation carried out by comparing

exclusively the agreement of the experimental and simulation particle fluxes, that is $Q \leq 0.25$.

IV. CONCLUSIONS

In the present paper, we discuss the methodology for carrying out a V&V procedure to make progress in the understanding of plasma turbulence. Rigorous techniques have been introduced to assess the correct implementation of the model equations in a simulation code (code verification), and estimate the numerical error affecting the simulation results (solution verification). The assessment of the agreement between experiments and simulations (validation) makes use of a number of validation observables to obtain a global metric χ normalized in order to be equal to 0 in the case of perfect agreement and 1 in the case of complete disagreement. A validation is not concluded until the quality of the comparison, Q , is also provided. The parameter Q is an index that can be used to compare validations among them; it reveals how well a comparison has been made, indicating the number of observables used for the comparison and how constraining they are.

The proposed methodology has been tested on the simulation of the basic plasma physics experiment TORPEX, focusing on measurements from Langmuir probes. We have considered simulations carried out with the GBS code, focusing on a two-dimensional and two three-dimensional models. The value of χ and Q are displayed in Fig. 4.

What progress has our V&V exercise allowed? First, by carrying out the verification procedure, we have largely increased our confidence on the GBS simulation results. In fact, we have rigorously shown that the drift-reduced model is correctly implemented in GBS and, by establishing a methodology to evaluate the magnitude of the numerical error affecting the simulation results, we have quantified the numerical uncertainty of the TORPEX simulations. Second, by comparing different models, we have made progress in the understanding of plasma turbulence in TORPEX. As discussed in Ref. 23, there are two turbulent regimes in TORPEX, each primarily driven by a distinct plasma instability: the ideal and the resistive interchange modes. The most obvious difference between the two regimes is the wave number along the magnetic field: $k_{\parallel} = 0$ in the ideal interchange case, while $k_{\parallel} \neq 0$ in the resistive case. The main parameter that controls the transition from one

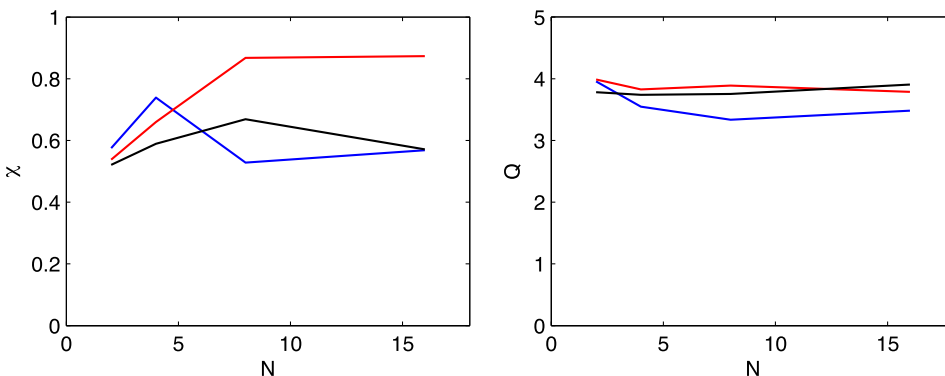


FIG. 4. Global metric, χ , and quality of the comparison, Q , for the TORPEX simulations as a function of N . The three-dimensional simulations with ad hoc boundary conditions (blue), the three-dimensional simulations with first-principle boundary conditions (black), and two-dimensional simulations (red) are considered.

instability to the other is the pitch of the field line, expressed in terms of the number of field line turns, N . At low values of N , TORPEX dynamics is dominated by the ideal interchange regime. Theoretical investigations²³ show that the transition to the resistive regime occurs at a value of N that depends on the plasma resistivity and on the vertical size of the device. At the TORPEX resistivity and size, the transition is expected to take place at $N \simeq 10$ as it is confirmed experimentally⁴⁴ and by the three-dimensional simulations, which show a transition between the two regimes while passing from the $N = 4$ to the $N = 8$ simulations. The validation exercise points out that it is essential to model correctly the transition from the ideal to the resistive interchange mode regime that has $k_{\parallel} \neq 0$ (not allowed in the two-dimensional simulations), in order to describe the plasma dynamics at high N .

The validation has also pointed out that no significant improvement in the description of the experimental results is made by the implementation of the first-principle set of boundary conditions. However, its implementation eliminates the need of a sensitivity analysis to the boundary conditions, and the possibility of a fortuitous agreement between simulations and experiments. On the other hand, it has been pointed out that the effect of the boundary conditions is particularly important in the parallel velocity profile.⁴⁵ We therefore expect that it would be possible to discriminate better the physics of the boundary conditions by considering observables that provide insights on the parallel flow and are based on measurements taken in proximity of the wall. As a matter of fact, the missing elements in the description of the T_e scale length and responsible for the underestimation of the fluctuation amplitude should be searched elsewhere (e.g., source nonlinearities, Boussinesq approximation, and presence of fast electrons). The importance of these elements can still be assessed through the use of the validation methodology. The example we provide shows that it is relatively easy to use this methodology to discriminate among models and assess whether or not they follow the right trend, pinpointing that the correct physics is described by them. On the other hand, it is much more delicate to judge a single model in absolute terms and to assess its predictive capabilities.

ACKNOWLEDGMENTS

The simulations presented herein were carried out at the Swiss National Supercomputing Centre (CSCS), under Project ID s346, and at the Computational Simulation Centre of the International Fusion Energy Research Centre (IFERCCSC), Aomori, Japan, under the Broader Approach collaboration between Euratom and Japan, implemented by Fusion for Energy and JAEA. This work was carried out within the framework of the EUROfusion Consortium. It was supported by the Swiss National Science Foundation and received funding from the European Unions Horizon 2020 research and innovation programme under Grant Agreement No. 633053. The views and opinions expressed herein do not necessarily reflect those of the European Commission.

APPENDIX A: THE EXPERIMENTAL SETUP

The considered experiments are performed in TORPEX, a toroidal device with major radius $R = 1$ m and minor radius $a = 0.2$ m. The vertical and toroidal components of the magnetic field create helicoidal field lines that terminate on the torus vessel. A hydrogen plasma is produced and sustained by microwaves in the electron cyclotron (EC) range of frequencies (a microwave power of 300 W is used in the experiments described here). Using the technique discussed in Ref. 46, it is observed that the plasma production is localized at the EC and upper hybrid (UH) layers, which are vertically elongated approximately around $r = -13$ cm and $r = -2$ cm, respectively.

A toroidal magnetic field $B_{\phi} = 76$ mT on axis is used, with four values of vertical magnetic field, $B_z = 2.4, 1.2, 0.6,$ and 0.3 mT. This results in $N = 2, 4, 8,$ and 16 turns of a magnetic field line in the device. Typical plasma parameters are in the range $n \simeq 10^{16}$ m⁻³, $T_e \simeq 5$ eV, $T_i \ll T_e$.

Diagnostics of the plasma dynamics used here include: (a) the SLP array, a linear array of 8 Langmuir probes, with 1.8 cm distance between tips, used to obtain most of the experimental results showed here; (b) the HEX TIP array, a two-dimensional hexagonal Langmuir probe array covering the whole poloidal cross section, with spatial resolution of 3.5 cm,⁴⁷ used to obtain the k_z measurements; (c) TWIN, two identical Langmuir probes, separated toroidally by 180 degrees, used to obtain the measurement of the toroidal mode number. A discussion on the interpretation of Langmuir probe data together with experimental consideration relative to the TORPEX device can be found in Ref. 48.

APPENDIX B: THE SIMULATION MODELS

Owing to the low TORPEX plasma temperature, the drift-reduced Braginskii equations (see, e.g., Ref. 35) can be used to model the TORPEX plasma dynamics. In the limit of $T_i \ll T_e$ and $\beta \ll 1$, and assuming that $B_z \ll B_{\phi}$ so that $B \simeq B_0 R / (R + r)$, since the magnetic curvature is constant along a field line and equal to $R + r$, these equations can be written as

$$\frac{\partial n}{\partial t} = \frac{c}{B} [\phi, n] + \frac{2c}{eRB} \left(\frac{\partial p_e}{\partial z} - en \frac{\partial \phi}{\partial z} \right) - \frac{\partial (nV_{\parallel e})}{\partial x_{\parallel}} + S_n, \quad (\text{B1})$$

$$\begin{aligned} \frac{\partial \nabla_{\perp}^2 \phi}{\partial t} &= \frac{c}{B} [\phi, \nabla_{\perp}^2 \phi] - V_{\parallel i} \frac{\partial \nabla_{\perp}^2 \phi}{\partial x_{\parallel}} + \frac{2B}{cm_i R n} \frac{\partial p_e}{\partial z} \\ &+ \frac{m_i \Omega_{ci}^2}{e^2 n} \frac{\partial j_{\parallel}}{\partial x_{\parallel}}, \end{aligned} \quad (\text{B2})$$

$$\begin{aligned} \frac{\partial T_e}{\partial t} &= \frac{c}{B} [\phi, T_e] + \frac{4c}{3eRB} \left(\frac{7}{2} T_e \frac{\partial T_e}{\partial z} + \frac{T_e^2}{n} \frac{\partial n}{\partial z} - e T_e \frac{\partial \phi}{\partial z} \right) \\ &+ \frac{2T_e}{3en} 0.71 \frac{\partial j_{\parallel}}{\partial x_{\parallel}} - \frac{2}{3} T_e \frac{\partial V_{\parallel e}}{\partial x_{\parallel}} - V_{\parallel e} \frac{\partial T_e}{\partial x_{\parallel}} + S_T, \end{aligned} \quad (\text{B3})$$

$$\frac{\partial V_{\parallel i}}{\partial t} = \frac{c}{B} [\phi, V_{\parallel i}] - V_{\parallel i} \frac{\partial V_{\parallel i}}{\partial x_{\parallel}} - \frac{1}{nm_i} \frac{\partial p_e}{\partial x_{\parallel}}, \quad (\text{B4})$$

$$m_e n \frac{\partial V_{\parallel e}}{\partial t} = m_e n \frac{c}{B} [\phi, V_{\parallel e}] - m_e n V_{\parallel e} \frac{\partial V_{\parallel e}}{\partial x_{\parallel}} \quad (\text{B5})$$

$$-T_e \frac{\partial n}{\partial x_{\parallel}} + en \frac{\partial \phi}{\partial x_{\parallel}} - 1.71 n \frac{\partial T_e}{\partial x_{\parallel}} + \frac{en}{\sigma_{\parallel}} j_{\parallel},$$

where $p_e = nT_e$, $[a, b] = \partial_r a \partial_z b - \partial_z a \partial_r b$, $j_{\parallel} = en(V_{\parallel i} - V_{\parallel e})$, $\Omega_{ci} = eB/(m_i c)$, and S_n and S_T are the density and temperature sources. The r coordinate denotes the radial direction, x_{\parallel} is parallel to B , and z is the direction perpendicular to r and x_{\parallel} (for $B_z \ll B_{\phi}$ the vertical and z directions are approximately the same).

The computational domain has an annular shape with a cross section $r = -L_v/2$ to $r = L_v/2$ and $z = 0$ to $z = L_v$. At $r = -L_v/2$ and $r = L_v/2$, Dirichlet boundary conditions are used for ϕ and $\nabla_{\perp}^2 \phi$ and Neumann boundary conditions for n , T_e , $V_{\parallel e}$, and $V_{\parallel i}$.

At the upper and lower walls, at $z=0$ and $z=L_v$, we consider two sets of boundary conditions. First, we implement an ad hoc set of boundary condition, where we impose $V_{\parallel i} = \pm c_s$ and $V_{\parallel e} = \pm c_s \exp(\Lambda - e\phi/T_e)$ with $\Lambda = \log \sqrt{m_i/(2\pi m_e)}$, $c_s = \sqrt{T_e/m_i}$, and we explore both Dirichlet and Robin boundary conditions for n and T_e , while for ϕ we use both Dirichlet boundary conditions $e\phi = \Lambda T_e$ (implying $V_{\parallel e} = V_{\parallel i}$) and a boundary condition of the form $\partial_z \phi \propto (e\phi - \Lambda T_e)$. Second, we use the first principle set of boundary conditions that has been derived in Ref. 24, that is $V_{\parallel i} = \pm c_s$, $V_{\parallel e} = \pm c_s \exp(\Lambda - e\phi/T_e)$, $\partial_z T_e = k_T \partial_z \phi$, $\partial_z n = \mp (n/c_s) \partial_z V_{\parallel i}$, $\omega = -\cos^2 \alpha [(\partial_z V_{\parallel i})^2 \pm c_s \partial_z^2 V_{\parallel i}]$, and $\partial_z \phi = \mp c_s \partial_z V_{\parallel i}$.

We have used source profiles that mimic the EC and UH resonance layer in TORPEX, i.e., $S_{n,T} = S_{0,n,T} \{S_{UH} \exp[-(r - r_{UH})^2/\lambda_{UH}^2] + S_{EC} \exp[-(r - r_{EC})^2/\lambda_{EC}^2]\}$, with $S_{UH} = 1.5$, $S_{EC} = 1$, $\lambda_{UH} = 1$ cm, $\lambda_{EC} = 0.5$ cm, $r_{UH} = -2$ cm, $r_{EC} = -6$ cm, and values of the source strength ($S_{0n} = 1.5 \times 10^{20} \text{ m}^{-3} \text{ s}^{-1}$, $S_{0T} = 3.5 \times 10^4 \text{ eV/s}$) estimated experimentally through a global balance of the TORPEX plasma. We remark that dependence of the UH resonance position on n is neglected in the present model. Other values used are: $R = 1$ m, $L_v = 40$ cm, $m_i/m_e = 200$, and $\Lambda = 3$, the resistivity has been varied, ranging from $\nu = 0.01 c_s/R$ to $\nu = 1 c_s/R$, in order to check the influence of this parameter.

GBS solves Eqs. (B1)–(B5) on a field-aligned grid using a second-order finite difference scheme with Runge-Kutta time stepping and small diffusion terms. The Poisson bracket is evaluated by using the Arakawa scheme.

If only $k_{\parallel} \simeq 0$ modes are considered, simple two-dimensional fluid equations that describe the plasma turbulence can be considered. The Braginskii equations are integrated in the parallel direction in order to evolve the line-integrated density, $n(r, z) = \int n(r, z, x_{\parallel}) dx_{\parallel}/L_c$, potential, $\phi(r, z) = \int \phi(r, z, x_{\parallel}) dx_{\parallel}/L_c$, and temperature, $T_e(r, z) = \int T_e(r, z, x_{\parallel}) dx_{\parallel}/L_c$, $L_c = 2\pi NR$ being the magnetic field line length. We use Bohm's boundary conditions to take into account the ion and electron parallel flow at the sheath edge: by assuming that the density at the edge is equal to $n(r, z)/2$, it is possible to approximate the ion and electron flows as $\Gamma_{\parallel i} = nc_s/2$ and $\Gamma_{\parallel e} = nc_s \exp(-e\phi/T_e + \Lambda)/2$. The evolution equations for n , ϕ , and T_e thus become

$$\frac{\partial n}{\partial t} = \frac{c}{B} [\phi, n] + \frac{2c}{eRB} \left(\frac{\partial p_e}{\partial z} - en \frac{\partial \phi}{\partial z} \right) - \frac{\sigma c_s}{R} \exp(\Lambda - e\phi/T_e) + S_n, \quad (\text{B6})$$

$$\frac{\partial \nabla^2 \phi}{\partial t} = \frac{c}{B} [\phi, \nabla^2 \phi] + \frac{2B}{cm_i R n} \frac{\partial p_e}{\partial z} + \frac{\sigma c_s m_i \Omega_i^2}{eR} [1 - \exp(\Lambda - e\phi/T_e)], \quad (\text{B7})$$

$$\frac{\partial T_e}{\partial t} = \frac{c}{B} [\phi, T_e] + \frac{4c}{3eRB} \left(\frac{7}{2} T_e \frac{\partial T_e}{\partial z} + \frac{T_e^2}{n} \frac{\partial n}{\partial z} - eT_e \frac{\partial \phi}{\partial z} \right) - \frac{2}{3} \frac{\sigma T_e c_s}{R} [1.71 \exp(\Lambda - e\phi/T_e) - 0.71] + S_T, \quad (\text{B8})$$

where $\sigma = R/L_c = 1/(2\pi N)$. We note that a similar system of equations has been used in Ref. 49. The system of Eqs. (B6)–(B8) has been solved numerically, using the earliest version of GBS that has been developed from the ESEL code.⁵⁰ The algorithm used is described in Ref. 51.

For the two dimensional simulations, we consider a domain with extension L_r in the radial direction and L_v/N along z . The boundary conditions are periodic along the vertical direction (due to the flute property of the interchange mode) and we use Dirichlet boundary conditions in the radial direction. In order to study the sensitivity of the results to the parallel boundary conditions, a scan of the σ parameter has been performed.

Both for the three-dimensional and the two-dimensional case, the simulation is started from random noise. Then, the sources introduce plasma and heat, increasing the plasma pressure and triggering the interchange instability. The interchange instability leads to density and particle transport in the radial direction from the source region to the low field side of the machine. At the same time, plasma is removed from the system by parallel losses. The results discussed in the present paper focus on the quasi-steady-state period, established after the initial simulation transient, as a result of a balance between parallel losses, perpendicular transport, and sources.

A detailed analysis of the plasma dynamics described by the three-dimensional model (B1)–(B5) has been presented in Refs. 22 and 23, while the simulation results obtained from the two-dimensional model (B6)–(B8) has been discussed in Ref. 25.

¹W. L. Oberkampf and T. G. Trucano, *Prog. Aerosp. Sci.* **38**, 209 (2002).

²W. L. Oberkampf and C. J. Roy, *Verification and Validation in Scientific Computing* (Cambridge University Press, New York, NY, USA, 2010).

³P. J. Roache, *Verification and Validation in Computational Science and Engineering* (Hermosa Publishers, Albuquerque, NM, USA, 1998).

⁴A. M. Dimits, G. Bateman, M. A. Beer, B. I. Cohen, W. Dorland, G. W. Hammett, C. Kim, J. E. Kinsey, M. Kotschenreuther, A. H. Kritiz, L. L. Lao, J. Mandrekas, W. M. Nevins, S. E. Parker, A. J. Redd, D. E. Shumaker, R. Sydora, and J. Weiland, *Phys. Plasmas* **7**, 969 (2000).

⁵J. Birn, J. F. Drake, M. A. Shay, B. N. Rogers, R. E. Denton, M. Hesse, M. Kuznetsova, Z. W. Ma, A. Bhattacharjee, A. Otto, and P. L. Pritchett, *J. Geophys. Res.* **106**, 3715, doi:10.1029/1999JA900449 (2001).

⁶P. Ricci, J. U. Brackbill, W. Daughton, and G. Lapenta, *Phys. Plasmas* **11**, 4102 (2004).

⁷V. Umansky, M. S. Day, and T. D. Rognlien, *Numer. Heat Transfer, Part B* **47**, 533 (2005).

- ⁸J. R. Myra, D. A. D'Ippolito, D. A. Russel, and M. Umansky, *Bull. Am. Phys. Soc.* **52**, 533 (2007).
- ⁹G. L. Falchetto, B. D. Scott, P. Angelino, A. Bottino, T. Dannert, V. Grandgirard, S. Janhunen, F. Jenko, S. Jolliet, A. Kendl, B. F. McMillan, V. Naulin, A. H. Nielsen, M. Ottaviani, A. G. Peeters, M. J. Pueschel, D. Reiser, T. T. Ribeiro, and M. Romanelli, *Plasma Phys. Controlled Fusion* **50**, 124015 (2008).
- ¹⁰R. V. Bravenec, Y. Chen, J. Candy, W. Wan, and S. Parker, *Phys. Plasmas* **20**, 104506 (2013).
- ¹¹S. Seiner and P. J. Roache, *J. Comput. Phys.* **57**, 251 (1985).
- ¹²P. J. Roache, *J. Fluids Eng.* **124**, 4 (2002).
- ¹³C. J. Roy, *J. Comput. Phys.* **205**, 131 (2005).
- ¹⁴P. J. Roache, *Annu. Rev. Fluid Mech.* **29**, 123 (1997).
- ¹⁵F. Stern, R. V. Wilson, H. W. Coleman, and E. G. Paterson, *J. Fluids Eng.* **123**, 793 (2001).
- ¹⁶P. J. Roache, *J. Fluids Eng.* **116**, 405 (1994).
- ¹⁷P. W. Terry, M. Greenwald, J.-N. Leboeuf, G. R. McKee, D. R. Mikkelsen, W. M. Nevins, D. E. Newman, D. P. Stotler, Task Group on Verification and Validation, U.S. Burning Plasma Organization, and U.S. Transport Task Force, *Phys. Plasmas* **15**, 062503 (2008).
- ¹⁸M. Greenwald, *Phys. Plasmas* **17**, 058101 (2010).
- ¹⁹A. Fasoli, B. Labit, M. McGrath, S. H. Muller, G. Plyushchev, M. Podesta, and F. M. Poli, *Phys. Plasmas* **13**, 055902 (2006).
- ²⁰A. Fasoli, A. Burckel, L. Federspiel, I. Furno, K. Gustafson, D. Iraj, B. Labit, J. Loizu, G. Plyushchev, P. Ricci, C. Theiler, A. Diallo, S. H. Muller, M. Podesta, and F. M. Poli, *Plasma Phys. Controlled Fusion* **52**, 124020 (2010).
- ²¹P. Ricci, F. D. Halpern, S. Jolliet, J. Loizu, A. Masetto, A. Fasoli, I. Furno, and C. Theiler, *Plasma Phys. Controlled Fusion* **54**, 124047 (2012).
- ²²P. Ricci and B. N. Rogers, *Phys. Plasmas* **16**, 092307 (2009).
- ²³P. Ricci and B. N. Rogers, *Phys. Rev. Lett.* **104**, 145001 (2010).
- ²⁴J. Loizu, P. Ricci, F. D. Halpern, and S. Jolliet, *Phys. Plasmas* **19**, 122307 (2012).
- ²⁵P. Ricci, B. N. Rogers, and S. Brunner, *Phys. Rev. Lett.* **100**, 225002 (2008).
- ²⁶P. Ricci and B. N. Rogers, *Phys. Plasmas* **16**, 062303 (2009).
- ²⁷P. Ricci, C. Theiler, A. Fasoli, I. Furno, B. Labit, S. H. Muller, M. Podesta, and F. M. Poli, *Phys. Plasmas* **16**, 055703 (2009).
- ²⁸P. Ricci, C. Theiler, A. Fasoli, I. Furno, B. Labit, K. Gustafson, D. Iraj, and J. Loizu, *Phys. Plasmas* **18**, 032109 (2011).
- ²⁹F. Riva, P. Ricci, F. D. Halpern, S. Jolliet, J. Loizu, and A. Masetto, *Phys. Plasmas* **21**, 062301 (2014).
- ³⁰L. F. Richardson, *Philos. Trans. R. Soc., A* **210**, 307 (1911).
- ³¹L. F. Richardson and J. A. Gaunt, *Philos. Trans. R. Soc., A* **226**, 299 (1927).
- ³²P. J. Roache and P. M. Knupp, *Commun. Numer. Methods Eng.* **9**, 365 (1993).
- ³³S. A. Richards, *Commun. Numer. Methods Eng.* **13**, 573 (1997).
- ³⁴R. H. Myers, D. C. Montgomery, and C. M. Anderson-Cook, *Response Surface Methodology: Process and Product Methodology, Using Designed Experiment*, 3rd ed. (Wiley, 2009).
- ³⁵A. Zeiler, J. F. Drake, and B. Rogers, *Phys. Plasmas* **4**, 2134 (1997).
- ³⁶B. N. Rogers and P. Ricci, *Phys. Rev. Lett.* **104**, 225002 (2010).
- ³⁷P. Ricci and B. N. Rogers, *Phys. Plasmas* **20**, 010702 (2013).
- ³⁸A. Masetto, F. D. Halpern, S. Jolliet, J. Loizu, and P. Ricci, *Phys. Plasmas* **20**, 092308 (2013).
- ³⁹F. D. Halpern, P. Ricci, B. Labit, I. Furno, S. Jolliet, J. Loizu, A. Masetto, G. Arnoux, J. P. Gunn, J. Horacek, M. Kocan, B. LaBombard, C. Silva, and JET-EFDA Contributors, *Nucl. Fusion* **53**, 122001 (2013).
- ⁴⁰J. Loizu, P. Ricci, F. D. Halpern, S. Jolliet, and A. Masetto, *Plasma Phys. Controlled Fusion* **55**, 124019 (2013).
- ⁴¹C. Theiler, A. Diallo, A. Fasoli, B. Labit, M. Podesta, F. M. Poli, and P. Ricci, *Phys. Plasmas* **15**, 042303 (2008).
- ⁴²Wolfram Research, Inc., *Mathematica* (Champaign, Illinois, 2010).
- ⁴³S. H. Muller, A. Diallo, A. Fasoli, I. Furno, B. Labit, G. Plyushchev, M. Podesta, and F. M. Poli, *Phys. Plasmas* **13**, 100701 (2006).
- ⁴⁴F. M. Poli, P. Ricci, A. Fasoli, and M. Podesta, *Phys. Plasmas* **15**, 032104 (2008).
- ⁴⁵J. Loizu, P. Ricci, F. D. Halpern, S. Jolliet, and A. Masetto, *Phys. Plasmas* **21**, 062309 (2014).
- ⁴⁶M. Podesta, A. Fasoli, B. Labit, M. McGrath, S. H. Muller, and F. M. Poli, *Plasma Phys. Controlled Fusion* **48**, 1053 (2006).
- ⁴⁷S. H. Muller, A. Fasoli, B. Labit, M. McGrath, O. Pisaturo, G. Plyushchev, M. Podesta, and F. M. Poli, *Phys. Plasmas* **12**, 090906 (2005).
- ⁴⁸C. Theiler, I. Furno, A. Kuenlin, Ph. Marmillod, and A. Fasoli, *Rev. Sci. Instrum.* **82**, 013504 (2011).
- ⁴⁹N. Bisai, A. Das, S. Deshpande, R. Jha, P. Kaw, A. Sen, and R. Singh, *Phys. Plasmas* **11**, 4018 (2004).
- ⁵⁰V. Naulin, J. Nycander, and J. J. Rasmussen, *Phys. Rev. Lett.* **81**, 4148 (1998); O. E. Garcia, V. Naulin, A. H. Nielsen, and J. J. Rasmussen, *ibid.* **92**, 165003 (2004).
- ⁵¹V. Naulin and A. H. Nielsen, *SIAM J. Sci. Comput.* **25**, 104 (2003).